

Optical levitation using broadband light

A. T. M. Anishur Rahman* and P. F. Barker†

Department of Physics and Astronomy

University College London

Gower Street, WC1E 6BT London, UK

(Dated: May 20, 2022)

We demonstrate a novel and simple method for the creation of non-linear optical tweezer potentials using the chromatic aberration of a lens and the broadband output of a superluminescent diode. A tunable filter, typically used for ultra fast laser pulse shaping, allows us to shape the spectral profile and create tweezer potentials which are characterized by measuring the Brownian motion of levitated nanoparticles in vacuum. Finally, we show that interferometric detection and feedback cooling of the particle's motion can be achieved in this type of trap despite the low coherence of the trapping light.

I. INTRODUCTION

The creation of tailored optical tweezer potentials has become important across a wide range of fields from biology and rheology to atom optics and quantum science [1–9]. More recently, levitation of nanoparticles in vacuum using optical tweezers in combination with the control of the center-of-mass temperature has been used to explore quantum mechanics in a new high mass regime [10, 11]. Here the creation of well-controlled and rapidly modulated non-linear potentials is seen as a promising route to explore their quantum, non-classical motion.

Exquisite control over the phase and/or the amplitude of the light field, via spatial light modulators or digital mirror devices, has allowed the creation of complex optical potentials that can be changed over sub millisecond times scales[2–4, 7]. Other methods utilise rapid scanning of a single field to create time averaged tailored potentials [12]. These optical potentials are typically created by using a strong monochromatic laser which can be tightly focused due to its narrow linewidth and high spatial coherence. Traps constructed of broadband femtosecond laser sources with high peak intensities have also been used for optical tweezers [13] and they have been shown to have similar trapping efficiencies to those created by the cw lasers. In addition, the high peak intensities of the femtosecond laser, enhanced by the tweezer, have been shown to be useful for inducing non-linear optical properties [14–16]. Generally, however, broadband incoherent light sources are not considered to be useful for optical tweezers because they are typically of low intensity and are subject to chromatic aberration preventing the tight focusing required for the creation of deep optical potentials.

A superluminescent diode (SLD) is an intense, broadband light source produced by amplified spontaneous emission [17]. These devices have large linewidths that range from a few nanometers up to 100 nm and their low

coherence finds application in a large variety of applications including optical coherence tomography [18] and fiber optic gyroscopes [19]. Although SLDs have poor temporal coherence time, they have high transverse spatial coherence when coupled into a single mode fiber, allowing light to be focused to the small spot sizes required for optical trapping. Finally, as powers that exceed 100's of mW can be coupled into the fiber, there is sufficient power to form deep optical traps.

In this article, we demonstrate that the spectrally broad light of a superluminescent diode can be used to form deep and stable optical trapping potentials which are capable of levitating particles in vacuum. Additionally, we show that by filtering this light source using a tunable spectral filter constructed of grating pairs, that the inherent chromatic aberration of a typical lens allows us to produce a range of non-linear optical potentials. Finally, we show that parametric feedback cooling can be undertaken to control the center-of-mass temperature of a levitated particle and is as effective as that carried out by a laser.

II. OPTICAL POTENTIAL FROM A BROADBAND LIGHT SOURCE

The optical tweezers potential for subwavelength nanospheres is dominated by the dipole force which is determined by the intensity profile of the focused light beam $I(r)$, and the dielectric constant ϵ and volume V of the particle. The optical dipole potential in vacuum is given by $U(r) = -\frac{3V}{4c} \Re\left(\frac{\epsilon-1}{\epsilon+2}\right) I(r)$, where c is the speed of light in vacuum. The Gaussian spatial profile created by a focused laser beam produces a Gaussian potential well. However, when the energy of the particle is much less than the well depth it is very well approximated by a quadratic potential creating a simple harmonic oscillator in all three dimensions. The optical potential produced by a broadband source such as a superluminescent diode can be significantly different to that produced by a single mode laser since chromatic aberration due to dispersion in the focusing lens leads

* a.rahman@ucl.ac.uk

† p.barker@ucl.ac.uk

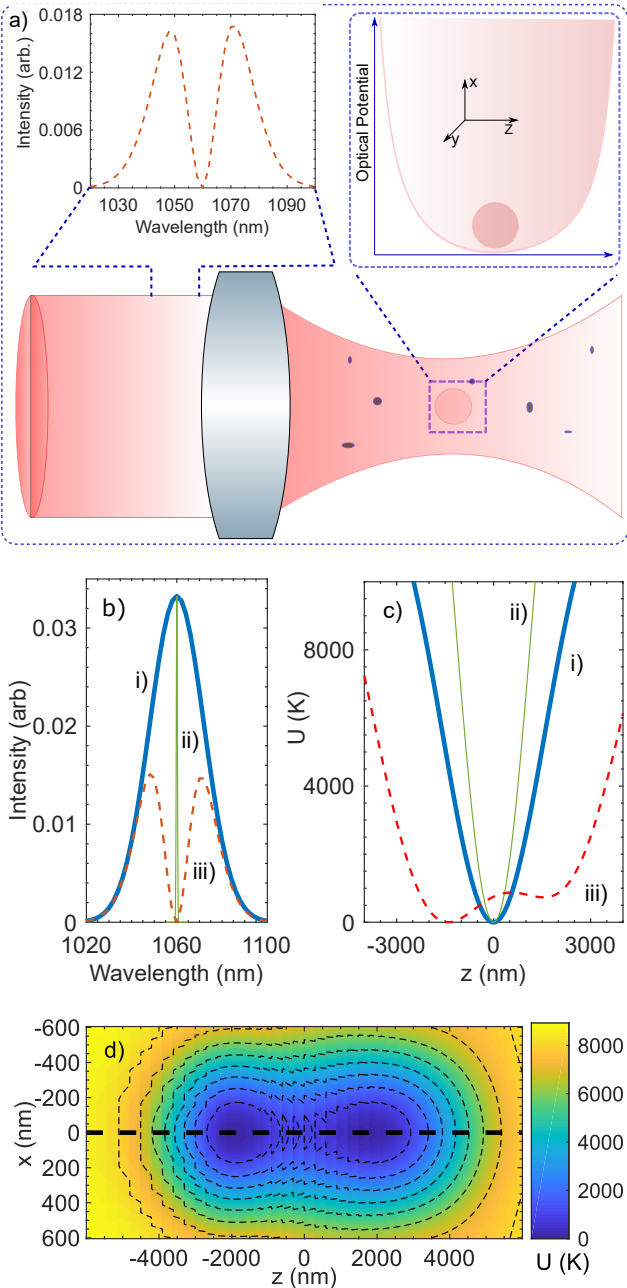


FIG. 1. a) A simplified experimental schematic where an aspheric lens made of lanthanum flint glass (D-ZLaF52LA) is used to form an optical tweezer trap for levitation. The left inset shows the spectral profile of the input light. The right inset is a sketch of the potential profile that can be generated using the chromatic aberration of the trapping lens and the filtered spectral profile of the trapping light (see text for details). b) Profiles produced by - i) a broadband light source with a linewidth of ≈ 28 nm, ii) a laser source and iii) a filtered profile obtained from the broadband source i). c) The potential wells associated with the spectral profiles of part b). The minima of all potential profiles have been set to zero for the purpose of comparison. d) The potential landscape in the x - z plane for the intensity profile iii of part b). The potential profile iii of part c) along the thick dashed black line. Contour lines are equipotentials. In calculating the potentials we use a silica nanosphere of $R = 50$ nm, a trapping power of 300 mW at the entrance of the lens, a lens diameter of 5 mm and a beam diameter of 8 mm at the entrance of the lens. The lens has a focal shift of 150 nm per 1 nm change in the wavelength.

to different focal lengths and focused spot sizes for each wavelength component. This is illustrated in figure 1a in which a high numerical aperture lens with chromatic aberration focuses a spectrally filtered broadband source such that at the focus a non-Gaussian or non-linear potential can be created. This is further highlighted in figure 1b and c which show three spectral profiles and their corresponding potentials calculated using the dispersion of a commercially available aspheric lens with a numerical aperture of $N.A.=0.77$ (D-ZLaF52LA, Edmund optics). The intensity profile is calculated using the Richards-Wolf formalism [20] and the contribution of all wavelength components is expressed as an incoherent sum as the interference terms between all of the different fields averages out to zero. Here the intensity is given by $I(r) = \frac{\epsilon_0 c}{2} \sum_{\lambda_{min}}^{\lambda_{max}} w_i (E_x(r, \lambda_i)^2 + E_y(r, \lambda_i)^2 + E_z(r, \lambda_i)^2)$, where w_i is the spectral weight, and $E_x(r, \lambda_i)$, $E_y(r, \lambda_i)$ and $E_z(r, \lambda_i)$ are the position and wavelength dependent optical field at position r around the focus of the trapping lens along the three major axes. The sum is taken over the range of wavelengths produced by the SLD which can be determined from a calibrated spectrometer. The focal length of the lens for each wavelength along the direction of light propagation (z -axis) is determined by the dispersion of the lens material, with a nominal effective focal length of 3.1 mm. Figure 1c shows the derived potentials in units of Kelvin (U/k_B), corresponding to the three experimentally feasible intensity profiles shown in Fig. 1b. Here, k_B is the Boltzmann constant. The minima of all potential profiles in Fig. 1c have been set to zero for the purpose of comparison. In the simulation we have used a $R = 50$ nm silica nanoparticle and a trapping power of 300 mW at the entrance of the trapping lens. Additionally, a focal shift of 150 nm per 1 nm in the trapping wavelength due to the dispersion of the lens material has been used. As expected, the optical potential produced by the broadband source with a linewidth of 28 nm (profile i) is much shallower than that produced by an ideal single mode laser source (profile ii) but is still deep enough ($> 10k_B T$ [20]) for trapping particles. This shallowness of the potential profile i arises from the fact that the each wavelength component that forms this potential focuses at a slightly different location along the z -axis creating a spread in the focus. Intensity profile iii in Fig. 1b, generated from the profile i using a notch filter, produces a double-well, albeit shallow, potential (profile iii, Fig. 1c). The formation of this potential can be understood from profile iii, in which there are effectively two spectral peaks. On focussing this light using a chromatically aberrated lens, two spatially separated focal spots are created which eventually form two potential wells. Here, the well near $z \approx -1700$ nm ($z \approx 2000$ nm) is associated with the peak centered around 1050 nm (1070 nm) (profile iii, Fig. 1b). The difference in the height between the minima of the two wells arises mainly from the tight (loose) focus and hence a higher intensity of the shorter (longer) wavelengths for the same optical power. In addition, the faster rise of the left boundary wall (see (profile iii, Fig.

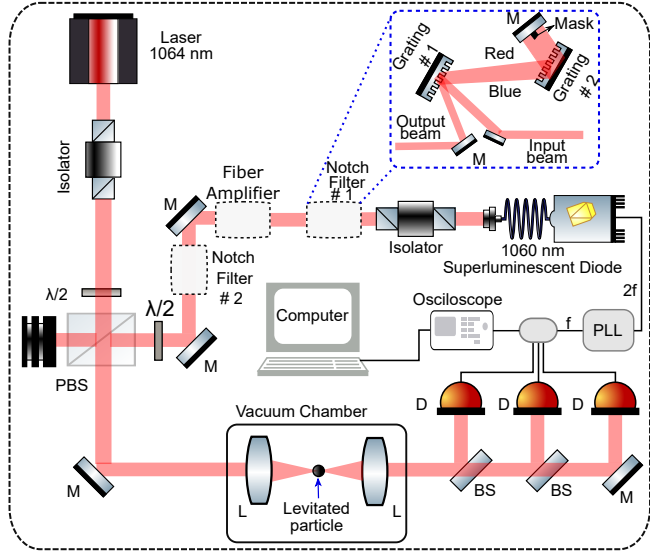


FIG. 2. Optical layout used for levitation. The labelled components are : $\lambda/2$ - half waveplate, M - mirror, BS - beam splitter, PBS - polarizing beam splitter, D - balanced photodiode and L - lens. Dotted lines represent components that are used for some of the experiments. Inset shows the home-built notch filter which consists of a beam block, a mirror and two identical gratings mounted parallel to each other. The linewidth and the center wavelength of the notch filter can be tuned by changing the width and the position of the block. For parametric feedback using the SLD, signals from the balanced photodiodes are fed to phase-locked loops (PLL). The output of the PLL, with suitable attenuation, is used as the input to the SLD current controller. See main text for more details.

1c) creating the asymmetry in the overall potential well is also due to the higher intensity of the light associated with the left well. Figure 1d shows a 2D plot of the potential landscape in the $x - z$ plane corresponding to the intensity profile *iii*, Fig. 1b. Two wells (blue areas) can be seen. The contour lines represent equipotentials. Polarization of the light was taken along the y -axis. As expected, the well on the left is more confined along both directions than that on the right consistent with Fig. 1c (profile *iii*). Profile *iii*, Fig. 1, is equivalent to the potential along the thick dashed black line in Fig. 1d. Overall, the spatial separation between the two wells (profile *iii*, Fig. 1c) and the height of the separating wall can be adjusted by using a wider notch filter (see below) and a higher optical power. Additionally, with an engineered twin-peak intensity profile that has a higher intensity in the peak centered around the longer wavelength, one can create a double-well potential which is a mirror image of the potential *iii* (simulation results not shown).

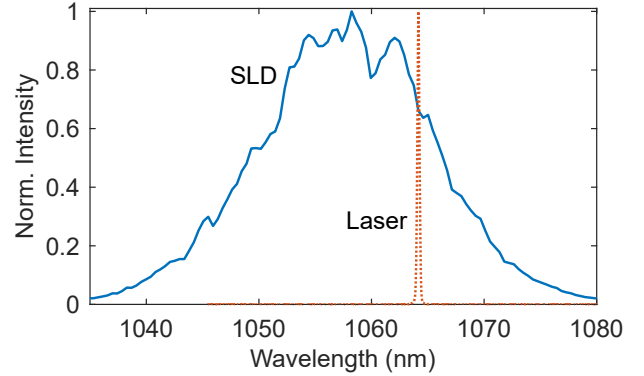


FIG. 3. The spectral profile of an unfiltered and unamplified superluminescent diode and a single mode Nd:YAG laser for comparison. Note that due to instrumental broadening the laser has a significantly narrower linewidth than indicated here.

III. EXPERIMENTAL SETUP

In our experiment an optical tweezers is formed using a 0.77 numerical aperture (NA) aspheric lens made of dense lanthanum flint glass (D-ZLaF52LA, part no. 83-674, Edmund Optics) with a focal length of 3.1 mm. The lens is housed inside a vacuum chamber as shown in Fig. 2 and levitation of silica nanospheres is carried using either a super luminescent diode or a Nd:YAG laser. The SLD wavelength is centered around 1060 nm and has a linewidth of 18 nm and is shown in Figure 3. The SLD does have a stable ripple structure indicating that it is not completely modeless. Also shown in Fig. 3 is the spectral profile of the 1064 nm Nd:YAG single mode laser output whose linewidth is significantly lower (≈ 10 kHz) than shown. The beams from each source are combined on a polarizing beam splitter (PBS) and propagate co-linearly into the trapping lens. To compensate for losses via spectral filtering, we use a fiber amplifier to amplify the beam up to a maximum of 1.4 W. The output power of the amplifier remains constant irrespective of the spectral profile of the input beam due to saturation of the amplifier gain. The tunable notch filter, which is used to create the non-linear optical potential, is discussed in more detail below. For some spectral profiles we can trap particles without the amplifier. Once levitated, we detect the particle's oscillatory motion in each trap axis using three balanced photodiodes [21, 22]. For parametric feedback cooling [21], the signals from the photodiodes are fed to a lock in amplifier where an oscillator is phase locked to each of the three trap frequency. The sum of the three oscillators is fed to the current controller of the super luminescent diode. This modulates the output of the SLD generating the signal for the parametric feedback cooling. Modulating the current directly means that we do not require an acousto/electro optic modulator [21, 23]. For typical operation, the modulation index of the intensity fluctuation of the SLD was less than 1%.

The SLD spectral profile is modified by a notch filter (see the inset, top right corner, Fig. 2) consisting of a retro-reflecting mirror and two identical blazed diffraction gratings (600 grooves/mm, Thorlabs Inc.) mounted parallel to each other. This arrangement is typically used for compression of pulses in chirp pulse amplification schemes [24]. To operate this filter, the spectrally broad trapping beam, as shown in Fig. 3, is collimated and directed towards the first grating. This spectrally dispersed and diverging beam from the first grating is directed onto a second grating which is arranged to prevent further spectral dispersion creating a collimated beam. In this beam, the wavelength components are spatially dispersed in the horizontal plane (see Fig. 2). To modify the spectral profile we place a mask in the beam which blocks the appropriate spectral components. The width (3 – 7 mm) of the mask determines the spectral contents removed from the beam while its position with respect to the beam fixes the centre wavelength of the notch filter. The filtered beam is then retroreflected by a mirror back through the grating pair where the spectral components are recombined into a collimated beam that can be used for trapping. The return beam is slightly displaced vertically with respect to the incoming beam and is picked off using a D-mirror as shown in figure 2. The return beam is then coupled into the optical amplifier to achieve the desired level of power for levitation.

IV. LEVITATION USING BROADBAND LIGHT

Nanoparticles were loaded into the trap by ultrasonic nebulization of silica nanoparticles dissolved in methanol at atmospheric pressure [21, 25]. The trapping power at the focus was approximately 150 mW from the superluminescent diode without any amplification or filtering. Once trapped, the chamber pressure was rapidly reduced down to a pressure of ≈ 5 mBar where the underdamped motion of the particles in the trap can be clearly resolved. At this pressure internal heating is not significant and the motional temperature of the particle can be well approximated by the room temperature value of 295 K [21, 23]. Figure 4a shows the averaged power spectral densities (PSD) of a 73 nm diameter silica nanoparticle (Corpuscular Inc.) levitated at 2 mBar. The graphs are an average of 66 PSDs taken over a duration of 10 seconds with a sampling rate of 1 MHz. The figures show that like laser based levitation [21–23, 26?–28], the oscillation frequency along the light propagation direction (z -axis) is the lowest while that in the direction (x -axis), orthogonal to the electric field polarization, is the highest. The difference in oscillation frequency between the x -axis and the y -axis (parallel to the direction of E field) is due to the asymmetry of the focus that occurs for non-paraxial focusing with a high NA lens [20]. Fig. 4b shows the histograms of position obtained from the time traces. As expected, the z -axis has the widest distribution due to the larger spot size

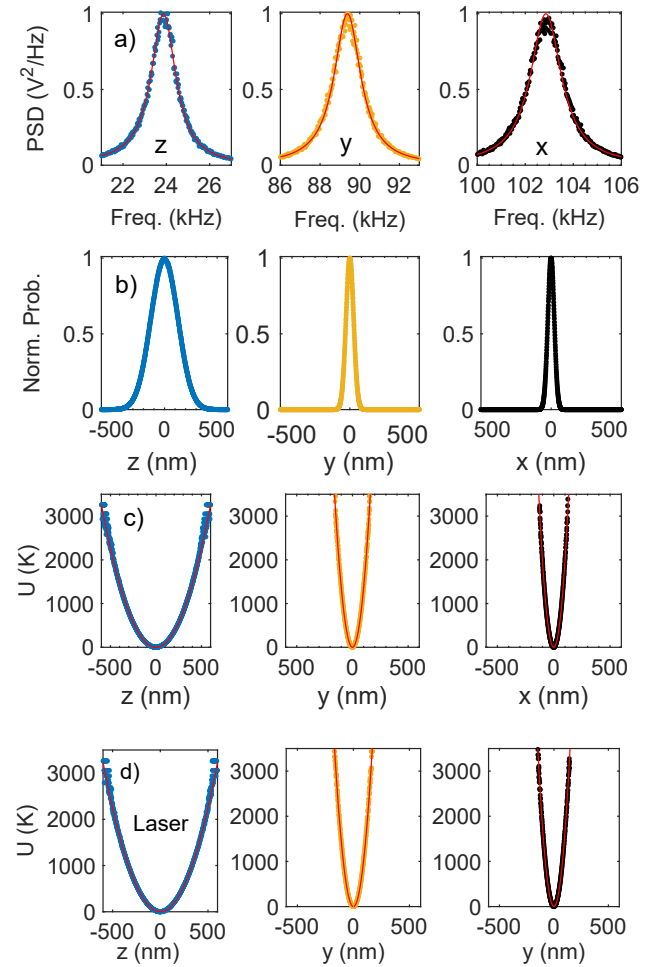


FIG. 4. Levitation using the superluminescent diode. a) The power spectral density along the three principle axes: z -axis represents the direction of light propagation, y -axis is parallel to the direction of the electric field (E) polarization and x -axis is perpendicular to E field polarization. b) The normalized position histograms along the three axes obtained from the calibrated time traces. c) The potential profiles derived from the position histograms. d) Potential profiles along the three axes from the same particle used in parts a-c but under the laser levitation. The frequency along the z -axis was purposely made equal to that under the SLD levitation, part a. This experiment was performed at ≈ 2 mBar. Red solid lines in parts c & d are quadratic functions. See main text for details.

along this direction, while the x -axis is the narrowest. A measurement of the position distribution can be used to reconstruct the potential assuming a Boltzmann distribution. That is, in thermal equilibrium, the probability of finding the levitated particle at position r is given by $p(r) \propto e^{-U(r)/k_B T}$, where k_B is the Boltzmann constant and T is the center-of-mass temperature. Provided that there are a statistically significant number of data points the potential can be determined as $U(r) \propto k_B T \ln p(r)$. Fig. 4c shows the relevant potential profiles along the three axes obtained using this procedure and that these

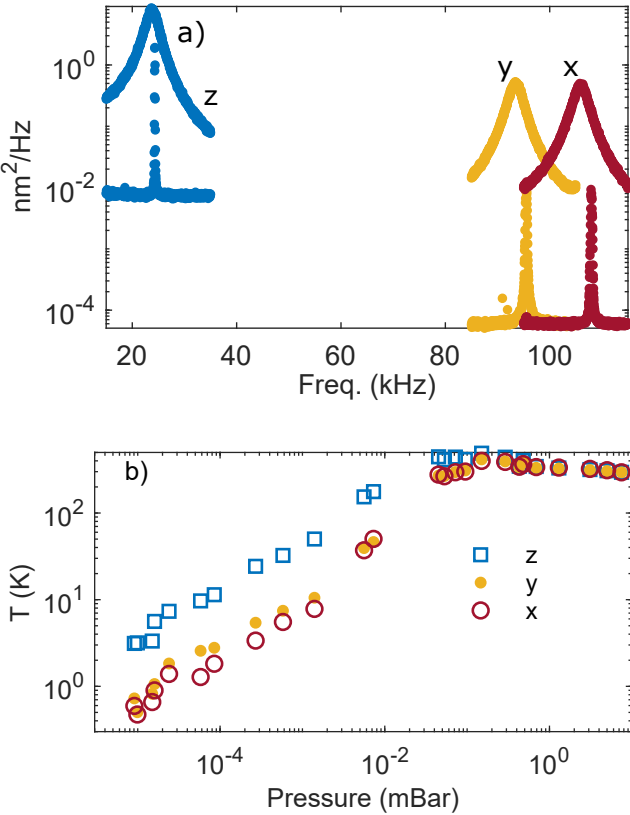


FIG. 5. Parametric feedback cooling using the SLD. a) Power spectral densities (PSD) along the three axes. The top graphs show PSDs at 5 mBar when no feedback is applied while the bottom graphs are the PSDs under parametric feedback cooling at $\approx 9 \times 10^{-6}$ mBar. b) Center-of-mass temperature along the three translational axes as a function of pressure under parametric feedback cooling.

match very well with the quadratic potential (solid red line). For comparison, in Fig. 4d, we show the potential profiles along the three axes when the same particle, used in Fig. 4a-c, is levitated using the laser. The trap frequency along the z -axis was purposely made equal to that under the SLD levitation (Fig. 4a). This means that the potential profiles in both cases are identical as can be observed from Figs. 4c&d. Here, to achieve the same trap frequency along the z -axis, SLD levitation requires 20% more power than laser levitation (100 mW at the focus). This extra trapping power to achieve the same trap frequency implies a spread in the focus along the z -axis. This confirms our simulation results shown in Fig. 1c, where under the same trapping power the superluminescent diode creates a shallower potential well and a lower trap frequency. Note that the trap frequencies along the x & y axes using the laser levitation (data are not shown) are lower than those under the SLD levitation. This is expected given that a lower laser trapping power was used [21].

V. PARAMETRIC FEEDBACK COOLING

Figure 5 shows the results of parametric feedback cooling [21] of the center-of-mass motion of a levitated nanoparticle under SLD levitation. In this case, light from the SLD without any filtering and amplification was used to trap the particle. Figure 5a shows the power spectral densities (PSD) along the three major axes. The top graphs are the PSDs before the feedback cooling is applied. The bottom graphs are with feedback on where the motional energy of the particle is significantly lower. Figure 5b shows the derived temperature of the particle along the three axes as a function of the residual gas pressure inside the vacuum chamber. Along all three axes the energy of the particle is reduced approximately by two orders of magnitude from the initial temperature (295 K). The lowest temperature of 470 mK along the x axis is reached at a pressure of 9×10^{-6} mBar. This is comparable to similar laser based cooling experiments [21, 23].

VI. LEVITATION WITH OPTICAL POTENTIAL CREATED BY THE FILTERED SLD

To demonstrate the creation of an anharmonic potential we now filter the broadband light from the SLD using the notch filter. Figure 6a shows one such intensity profile where the width of the notch filter was ≈ 10 nm. Fig. 6b shows the potential profile along the z -axis reconstructed from the position histogram as outlined above. Here, the black dots are the experimental data points. Asymmetry in the potential profile is immediately visible. In particular, the overall potential is tilted towards the right. At $|z| = 1350$ nm, the difference in the height between the two sides of the potential well is ≈ 980 K. To illustrate this anharmonicity, we fit a quadratic function (solid red line) to the experimental data. As expected, it deviates from the data points significantly. For a good fit, polynomials up to the 9th order (solid green line) are essential. This asymmetry arises due to the deep and the shallow potentials that the light created by the spectral peaks at 1058 nm and 1070 nm (Fig. 6a). In particular, the depth of each potential is roughly $\propto P/\lambda^2$, where P is the trapping power and λ is the wavelength of the trapping light. As a result, due to the higher (lower) power and the shorter (longer) wavelengths, light centered around 1058 nm (1070 nm) forms a tighter (shallower) trap. This means that the potential for $z < 0$ is expected to rise faster than for $z > 0$. Our simulation (blue dashed line) agrees qualitatively with the experimental data and discrepancies between the two can be attributed to our model which do not use the aspheric shape of the trapping lens but simply uses a focal length that changes with the lens dispersion. The inset in Fig. 6b shows the separate wells that the two peaks in the intensity profiles (Fig. 6a) would separately form. The potential well labeled with L is associated with the short

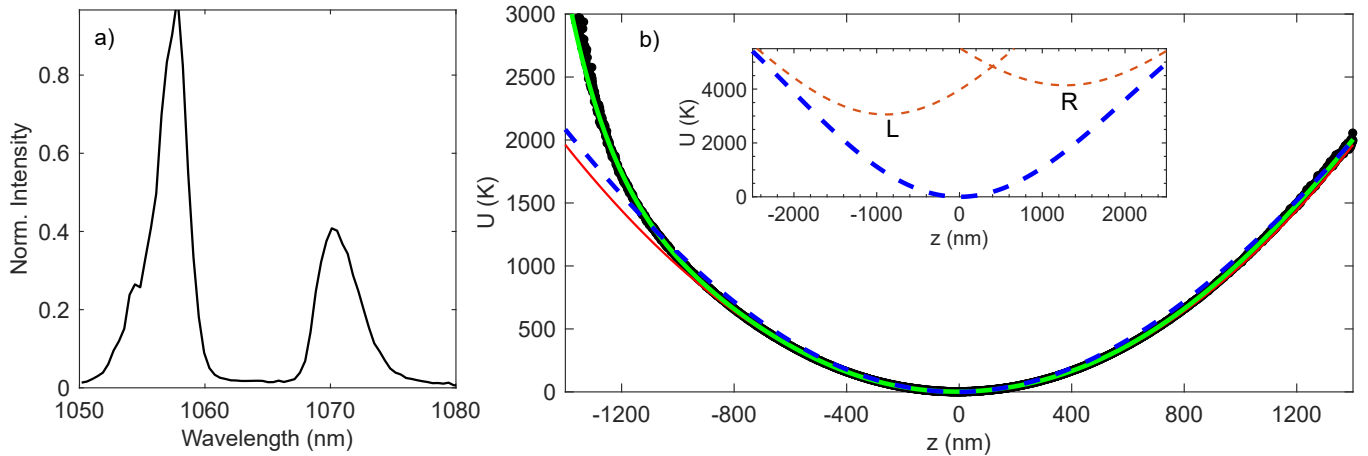


FIG. 6. Non-linear optical potential. a) SLD intensity profile after spectral filtering using a notch filter. b) Black dots are the experimental optical potential in unit of Kelvin. Experimental $U(z)$ has been obtained from the position histogram along z -axis. The red solid line represents a quadratic function while the blue dashed line is the simulation results obtained using the procedure described in Section 2. The green line is the function $f(z) = a_0 + a_1z + a_2z^2 + \dots + a_9z^9$, where the a_i s are constants. The inset shows the left (L) and right (R) wells that correspond to the peaks at 1058 nm and 1070 nm (part a) and their sum (blue dashed line). See main text for more details.

wavelength peak (1058 nm) and is deeper than the well R created by the long wavelength peak centered at 1070 nm.

VII. CONCLUSIONS

We have demonstrated optical levitation using a broadband superluminescent diode and have shown that this source can be used to form a deep optical harmonic potential that can be used for parametric feedback cooling of levitated nanoparticles. Importantly, by using the combination of an optical amplifier and a simple tunable notch filter, we can use the inherent chromatic aberration of the lens combined with the broadband nature of the light to create anharmonic potentials. These are limited only by the chromatic aberration in the lens and the spectral width of the superluminescent diode, both of which can be tuned to create the desired potential. Although,

not demonstrated here, both double well and quartic potentials appear feasible using lenses with higher aberration or by using a spectrally broader SLD source, both of which are currently commercially available. The mask of the tunable filter could be rapidly modulated in time using a digital mirror device while even more rapidly by electro-optic switching of the filter mask using a pockels cell. This would allow the potentials to be changed on submicrosecond timescales.

Acknowledgement: The authors acknowledge funding from the EPSRC Grant No. EP/S000267/1 and the Horizon 2020 program H2020-EU.1.2.1 TEQ project Grant agreement ID: 766900. The authors also acknowledge the help of J. Gosling in the laboratory.

[1] S. Fl̄ling, S. Trotzky, P. Cheinet, M. Feld, R. Saers, A. Widera, T. Mller, and I. Bloch, *Nature* **448**, 1029 (2007).

[2] M. Woerdemann, C. Alpmann, M. Esseling, and C. Denz, *Laser Photonics Rev.* **7**, 839 (2013).

[3] G. Gauthier, I. Lenton, N. M. Parry, M. Baker, M. J. Davis, H. Rubinsztein-Dunlop, and T. W. Neely, *Optica* **3**, 1136 (2016).

[4] D. Stuart and A. Kuhn, *New J. Phys.* **20**, 023013 (2018).

[5] *Opt. Commun.* **207**, 169 (2002).

[6] E. Schonbrun, R. Piestun, P. Jordan, J. Cooper, K. D. Wulff, J. Courtial, and M. Padgett, *Opt. Express* **13**, 3777 (2005).

[7] V. Boyer, R. M. Godun, G. Smirne, D. Cassettari, C. M. Chandrashekar, A. B. Deb, Z. J. Laczik, and C. J. Foot, *Phys. Rev. A* **73**, 031402 (2006).

[8] D. Preece, R. Warren, R. M. L. Evans, G. M. Gibson, M. J. Padgett, J. M. Cooper, and M. Tassieri, *J. Opt.* **13**, 044022 (2011).

[9] H. Zhang and K. Liu, *J. R. Soc. Interface* **5**, 671 (2008).

[10] F. Tebbenjohanns, M. Frimmer, V. Jain, D. Windey, and L. Novotny, *Phys. Rev. Lett.* **124**, 013603 (2020).

[11] U. Deli, M. Reisenbauer, D. Grass, V. Vuleti, N. Kiesel, and M. Aspelmeyer, *arXiv:1911.04406v2* (2019).

[12] A. Brut, A. Arakelyan, A. Petrosyan, S. Ciliberto, R. Dilenschneider, and E. Lutz, *Nature* **483**, 187 (2012).

[13] A. A. Ambadekar and Y. qing Li, *Opt. Lett.* **30**, 1797 (2005).

- [14] L. Gong, B. Gu, G. Rui, Y. Cui, Z. Zhu, and Q. Zhan, *Photon. Res.* **6**, 138 (2018).
- [15] Y. Jiang, T. Narushima, and H. Okamoto, *Nat. Phys.* **6**, 1005 (2010).
- [16] B. Agate, C. T. A. Brown, W. Sibbett, and K. Dholakia, *Opt. Express* **12**, 3011 (2004).
- [17] R. Cahill, P. P. Maaskant, M. Akhter, and B. Corbett, *Appl. Phys. Lett.* **115**, 171102 (2019).
- [18] T. H. Ko, D. C. Adler, J. G. Fujimoto, D. Mamedov, V. Prokhorov, V. Shidlovski, and S. Yakubovich, *Opt. Express* **12**, 2112 (2004).
- [19] K. Bhm, P. Marten, K. Petermann, E. Weidel, and R. Ulrich, *Electron. Lett.* **17**, 352 (1981).
- [20] L. Novotny and B. Hecht, *Principles of Nano-Optics*, 2nd ed. (Cambridge University Press, 2012) cambridge Books Online.
- [21] J. Gieseler, B. Deutsch, R. Quidant, and L. Novotny, *Phys. Rev. Lett.* **109**, 103603 (2012).
- [22] T. Li, S. Kheifets, and M. G. Raizen, *Nat. Phys.* **7**, 527 (2011).
- [23] J. Vovrosh, M. Rashid, D. Hempston, J. Bateman, M. Paternostro, and H. Ulbricht, *J. Opt. Soc. Am. B* **34**, 1421 (2017).
- [24] J. Agostinelli, G. Harvey, T. Stone, and C. Gabel, *Appl. Opt.* **18**, 2500 (1979).
- [25] F. Ricci, R. A. Rica, M. Spasenovi, J. Gieseler, L. Rondin, L. Novotny, and R. Quidant, *Nat. Commun.* **8** (2017).
- [26] A. T. M. A. Rahman, A. C. Frangescou, M. S. Kim, S. Bose, G. W. Morley, and P. F. Barker, *Sci. Rep.* **6** (2016).
- [27] A. T. M. A. Rahman and P. Barker, *Nature Photon* **11**, 634 (2017).
- [28] G. Ranjit, D. P. Atherton, J. H. Stutz, M. Cunningham, and A. A. Geraci, *Phys. Rev. A* **91**, 051805 (2015).